Electronic Supplementary Material (ESI) for Lab on a Chip.

Supplementary Information for "Multi-parametric functional imaging of cell cultures and tissues with a CMOS microelectrode array"

Jeffrey Abbott[1,2,3], Avik Mukherjee[4], Wenxuan Wu[1], Tianyang Ye[1,2], Han Sae Jung[1], Kevin M. Cheung[2], Rona S. Gertner[2], Markus Basan[4,*], Donhee Ham[1,*], and Hongkun Park[2,3,*]

[1]John A. Paulson School of Engineering and Applied Sciences, Harvard University, Cambridge, MA, USA.

[2]Department of Chemistry and Chemical Biology, Harvard University, Cambridge, Massachusetts, USA.

[3]Department of Physics, Harvard University, Cambridge, Massachusetts, USA.

[4]Department of System Biology, Harvard Medical School, Boston, Massachusetts, USA.

*To whom correspondence should be addressed: donhee@seas.harvard.edu and hongkun_park@harvard.edu; bio-related inquiries can be addressed to markus@hms.harvard.edu.

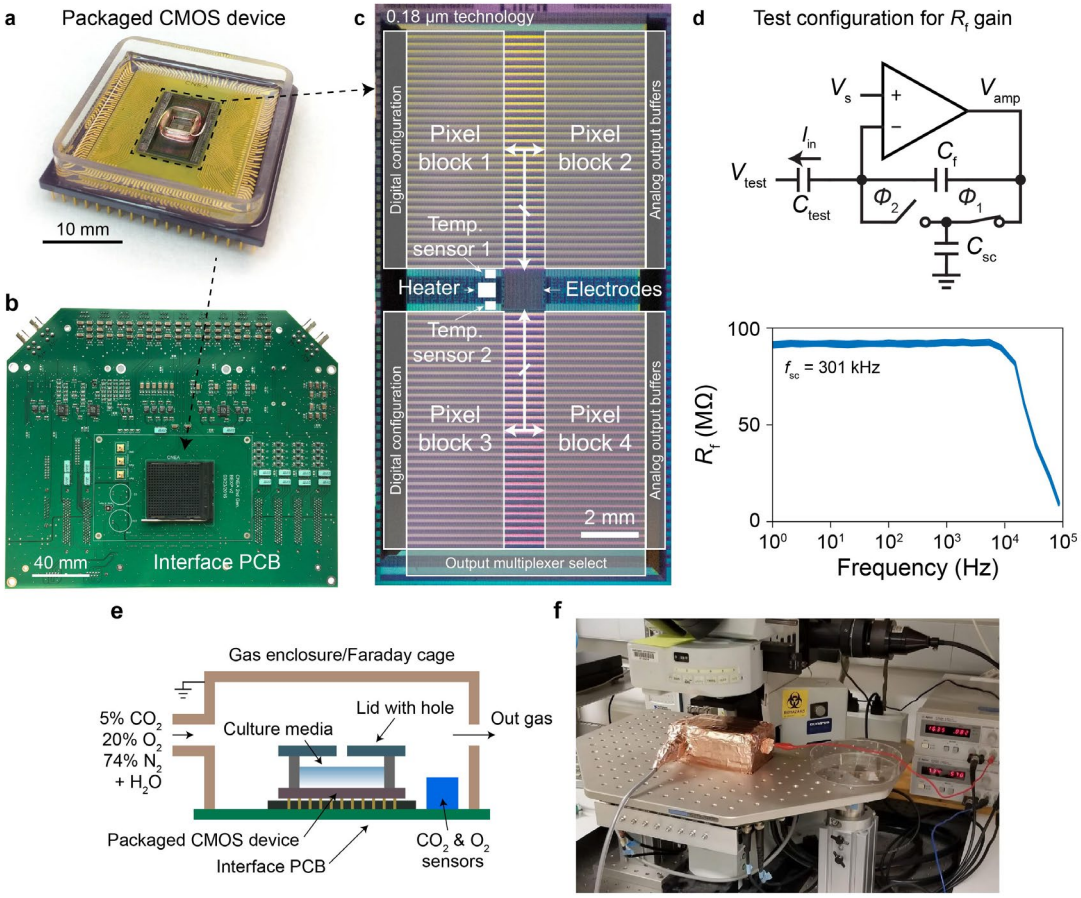

Supplementary Fig. 1 | Measurement setup for real-time electrical recordings. a-b, The CMOS device is packaged via wire bonding to a chip carrier (a) to electrically plug into an interface PCB (b) via backside pins. A microfluidic well for culturing cells is formed by attaching two glass rings to the CMOS IC and chip carrier via PDMS. PDMS is then poured between these two rings to encapsulate the wirebonds. **c**, The CMOS integrated circuit is fabricated in 0.18-µm technology occupying an area of 10 × 20 mm^2. An array of 64 × 64 = 4,096 electrodes at its center are connected to 4,096 pixel circuits (Fig. 1d) in the 4 peripheral quadrants (pixel blocks 1-4). For regulating cell culture temperature, a heater and two temperature sensors are included to the left of the electrode array. **d**, On-chip test measurement configuration (top) and transimpedance gain across frequency for 32 pixels (bottom). A clock of frequency 301 kHz with non-overlapping phases $\varphi_{1,2}$ drives the switched capacitance (C_{sc}) to create a 94 MΩ feedback resistance (R_f in Fig. 1d). A feedback capacitance (C_{sc}) of ~100 fF sets a bandwidth of ~30 kHz. A test capacitance (C_{test}) is used for current injection (I_{in}) for the measurement. **e**, A gas enclosure is placed over the device to improve cell viability during recordings. A combination of 5% CO_2 and air is run through a bubbler to increase humidity and form a mini incubator on the CMOS device with CO_2 and O_2 sensors on the interface PCB used for tuning. Temperature sensors and a heater integrated next to the electrode array regulate the device to 35-37ºC for recording. **f**, Image of the gas enclosure; the enclosure is covered in copper tape to block light and to form a Faraday cage.

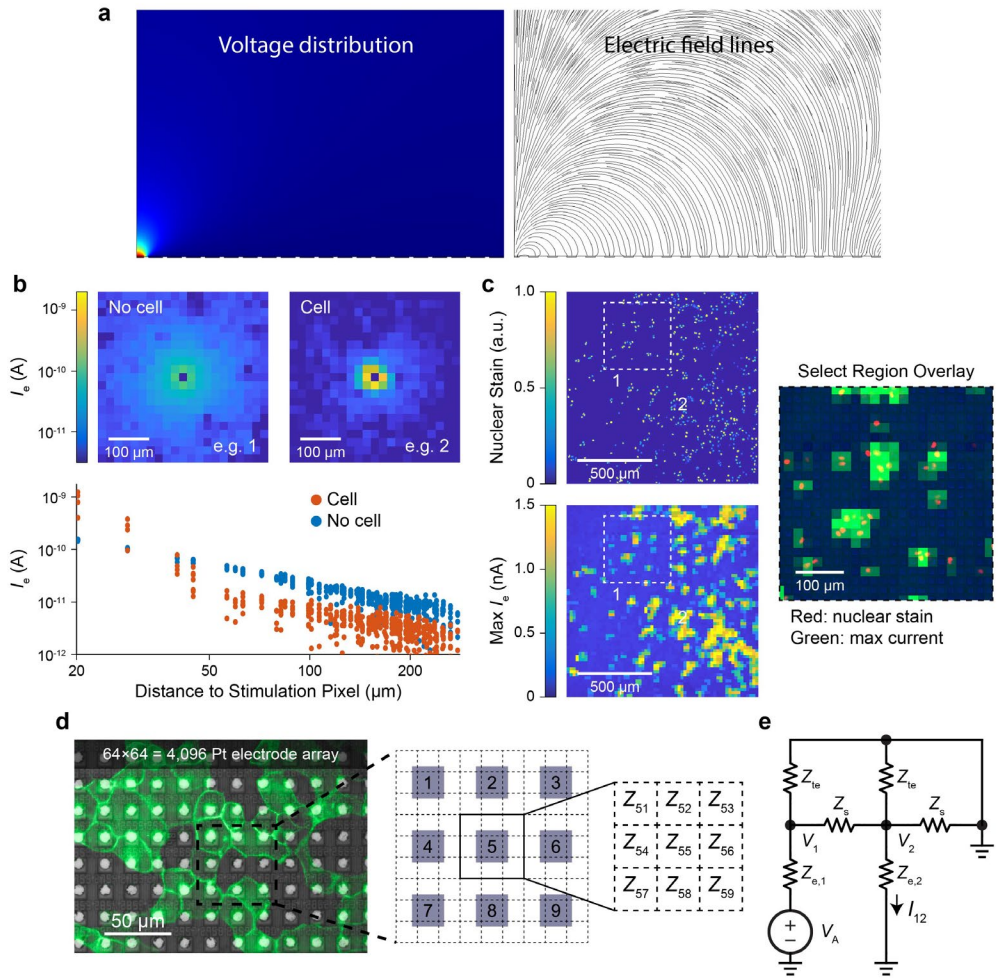

Supplementary Fig. 2 | Effect of attached cells on spatial current distribution over a CMOS electrode array. a, Cross-electrode measurement scheme simulation using COMSOL: applying an AC bias to one electrode while grounding the remaining electrodes creates fringing fields arcing high into the solution. A cell will affect the return distribution of the field lines that we measure using the transimpedance amplifiers in our CMOS integrated circuit (Fig. 2a). **b**, Measured electrode current (I_e) distribution heatmaps (top) of the nearest 11×11 recording electrodes for two stimulation electrodes without (e.g. 1) and with (e.g. 2) a MDCK cell. The I_e plotted versus distance (bottom) shows the cell increases the coupling to the nearest electrodes by almost an order of magnitude. **c**, Fluorescent image across the electrode array (top left) and a heatmap plot of the max I_e recorded for each stimulation electrode (bottom left). Overlay of a select region (right) of the nuclei fluorescence (red) and the max current (green). **d**, For higher spatial resolution and to map non-adherent cells, cross-electrode measurements are used to form a 3×3 impedance grid for each electrode. **e**, Circuit model used to calculate the cell-substrate impedance, Z_s, and transepithelial impedance, Z_{te}, for the application of an AC stimulation voltage, V_A, and a measurement of cross electrode current, I_{12}. The 3×3 impedance grid is used for the Z_s calculation while a single Z_{te} is extracted for each electrode. The electrode impedance, Z_e, can be calibrated out of both measurements (Supplementary Discussion 1).

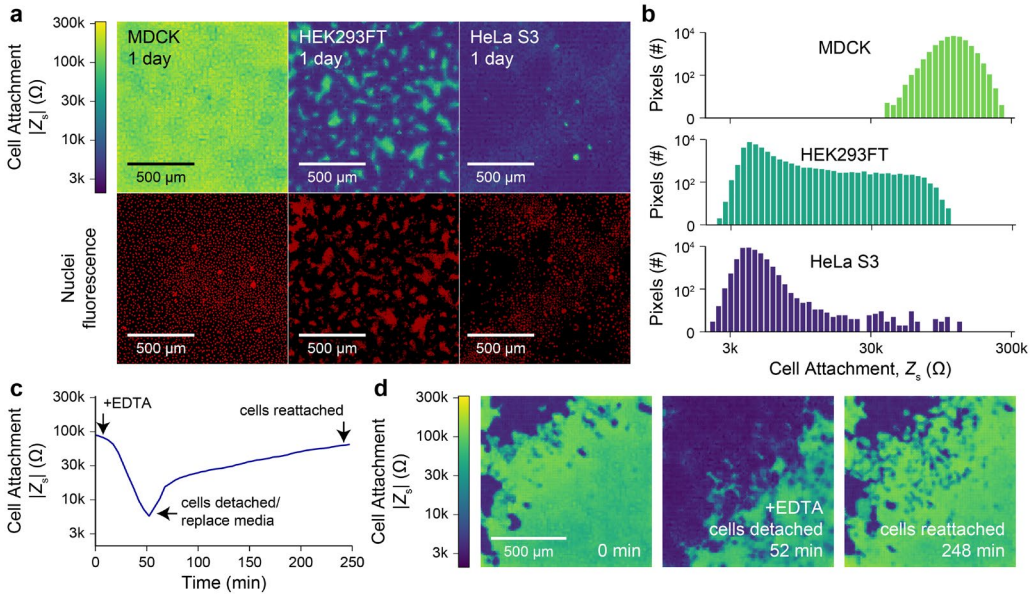

Supplementary Fig. 3 | Electrical mapping of cells using a CMOS electrode array. a, MDCK, HEK293FT, and HeLa S3 cell lines were plated uniformly at high densities and were electrically mapped via the cell attachment measurement (top) and optically imaged (bottom) with good spatial correspondence between the two measurements. **b**, Histograms of Z_s across the array for the three cell lines. **c-d**, Ethylenediaminetetraacetic acid (EDTA), a calcium chelator, was added to a MDCK cell culture at a final concentration of 5 mM to induce detachment with subsequent removal at 52 min to induce re-attachment. The mean Z_s value from the center of the array is plotted versus time in (**c**) and Z_s maps are plotted in (**d**) for three select times; a video of the time-course is shown in Supplementary Video 2.

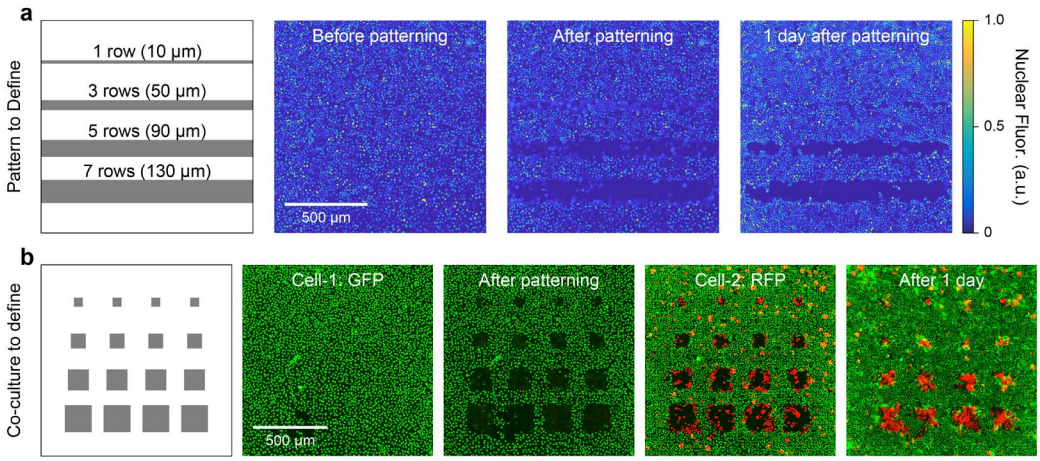

Supplementary Fig. 4 | Patterning for resolution testing and generation of co-cultures. a, Increasingly sized strips were used for testing the patterning resolution (left) using MDCK cells. No significant cell removal/death is observed after patterning for 1 row of electrodes, but three rows show significant cell death (blurred cells indicate cell death due to the collapse of the nucleus) attributed to the increased mass transport of the single electrode strips allowing for O_2 reduction to occur before H_2 gas generation. **b**, Various sized squares (minimum square of 3×3 electrodes) were used for patterning a co-culture (left). To pattern, a GFP expressing MDCK cell line (cell-1) was uniformly plated and fluorescently imaged. The cells were then patterned via a voltage application to generate H_2 gas. A RFP expressing MDCK cell line (cell-2) was then plated and partially filled the patterned areas. A confluent cell sheet formed after 1 day of culture reflecting the original pattern.

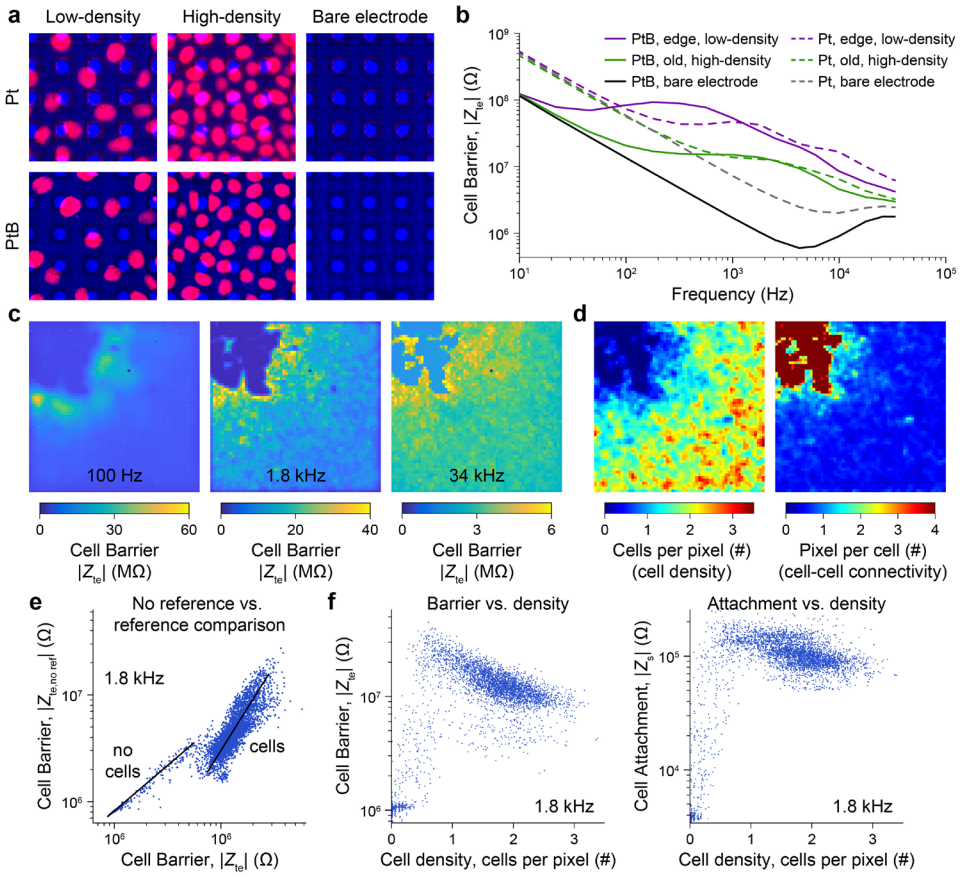

Supplementary Fig. 5 | Effects of platinum black and frequency on cell barrier sensitivity. a, Platinum black (PtB) was used to lower the electrode impedance, Z_e, to improve cell barrier measurement sensitivity. A comparison study (PtB culture is from Fig. 3) at ~72 hours with electrodes showing similar low-density, high-density, and without cells were used. **b**, The PtB lowered the Z_{te} measurement of bare electrodes by about 5×, allowing the cell-cell connections of the two different densities to be measured with higher signal-to-noise (Supplementary Discussion 1). **c**, Cell barrier maps versus a reference at different frequencies for the same culture as Fig. 3. The lower frequency measurements show more spread and do not capture the cell sheet edge but the 1.8 kHz measurement showed the highest contrast for the cell-connection measurement when compared to density maps extracted from imaging. **d**, Cell density and connectivity maps extracted from the nuclei of the fluorescence image of Fig. 3d. **e**, Comparison between Z_{te} measured without and with a reference at 1.8 kHz. Slightly smaller Z_{te} is measured without the reference, but for regions with cells and without (the two clusters) the relationship is direct. Measurements without the reference are preferred, as the Z_e contribution can be easily subtracted from the cell-substrate attachment measurement (Supplementary Discussion 1). **f**, Comparison between Z_{te} and Z_s versus extracted cell density (**d**) for the Fig. 3 experiment; Z_s is down-sampled via a bilinear interpolation to have the same spatial resolution as the Z_{te} measurement. The cell barrier shows a stronger dependence on cell density due to its measurement geared towards cell-cell connectivity. There is a small correlation between Zs and cell density as well, which can be seen from the cell-circuit model (Supplementary Fig. 2e) as having an effect if Z_s is high and the assumption that $Z_s << Z_{te}$ no longer holds which was used in the Z_s calculation (Supplementary Discussion 1).

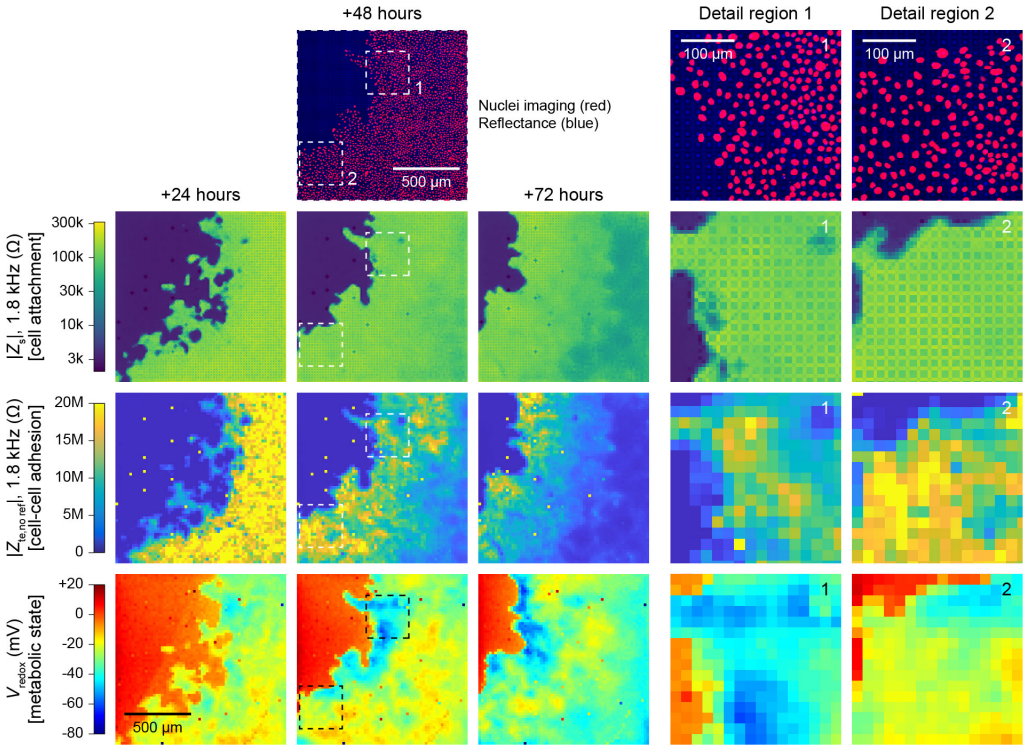

Supplementary Fig. 6 | Additional cell culture monitoring experiment showing similar characteristics to Fig. 3. Multi-parametric measurements of $|Z_s|$, $|Z_{te}|$, and V_{redox} at +24, +48, and +72 hours after MDCK cell plating to infer cell attachment, cell-cell adhesion, and metabolic state. Nuclei fluorescence imaging at 48 hours after plating (top) and a detail comparison of regions 1 & 2 (right) show correlation between cell density and cell-cell adhesion. The most negative redox potential is observed at the proliferation edge.

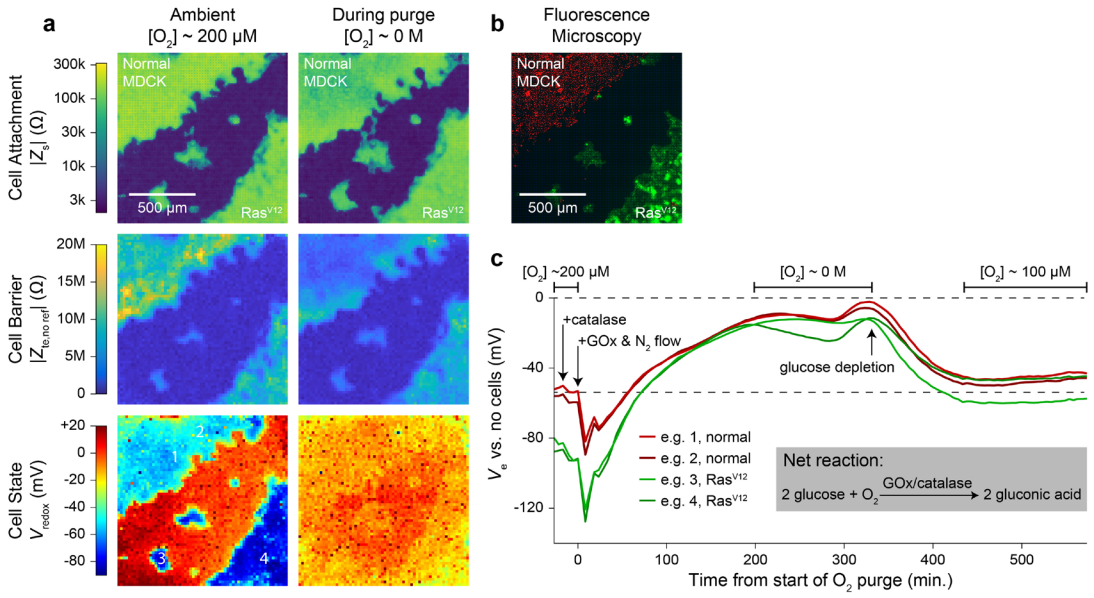

Supplementary Fig. 7 | Effects of an oxygen purge on normal and Ras^{V12} expressing MDCK cell tissue. a-c, An enzymatic and N_2-based O_2 purge was used to measure the effects of O_2 on the *in situ* extracellular redox potential for both MDCK (red nuclei in **b**, right) and Ras^{V12} expressing MDCK cells (green in **b**, right). Multi-parametric measurements are shown in (**a**) before and during the O_2 purge including cell attachment (top), cell barrier (middle), and cell state (bottom). Example pixel traces (**c**, e.g.'s 1-4 of both cell types) show a negative V_{redox} near the cells in comparison to without cells, indicating a more reducing environment with O_2 present, and the elimination of the negative potential with the O_2 purge. The more negative extracellular redox potential of the Ras^{V12} expressing cells is attributed to a more robust antioxidant environment. The normal MDCK cells also lose their cell barrier upon the O_2 related to their loss of structural polarity; the Ras^{V12} expressing cells showed little change as they did not exhibit strong cell-cell connectivity with O_2 present. Supplementary Video 6 shows full multi-parametric measurements of the purge experiment. A catalase concentration of 31 units/mL and a glucose oxidase concentration of 2 units/mL were used for the enzymatic purge.

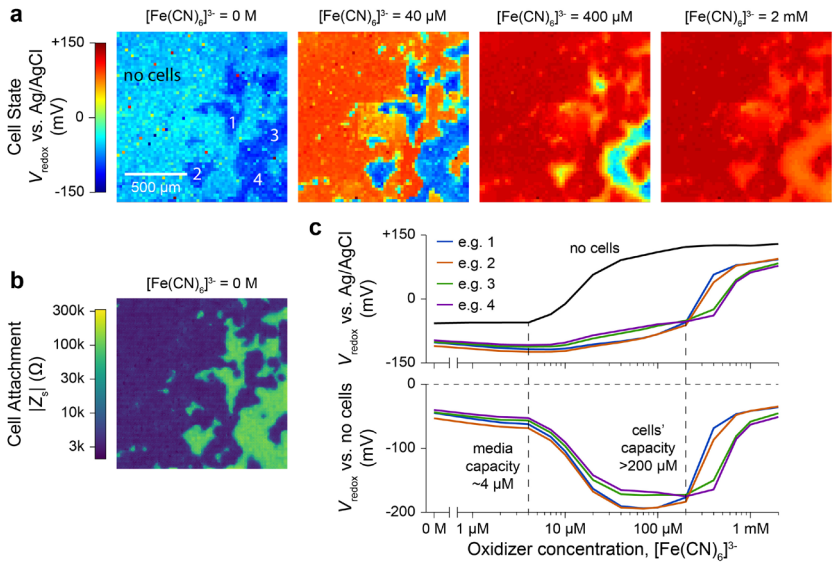

Supplementary Fig. 8 | Ferricyanide titration to determine reducing capacity of normal MDCK cells. **a-b**, Ferricyanide, $[Fe(CN)_6]^{3-}$, a membrane impermeable oxidizer, was titrated to 2 mM to measure the culture media and MDCK cells' reducing capacity via the *in situ* extracellular redox potential. Heatmaps of V_{redox} across the array before and during the titration are shown in (**a**) while a starting cell attachment map is shown in (**b**) for reference of the cells' locations. Supplementary Video 7 shows full multi-parametric measurements of the titration experiment. **c**, Titration curves for example pixels with cells, e.g.'s 1-4, and without cells versus a Ag/AgCl reference (**c**, top) and a relative measurement versus without cells (**c**, bottom) show the reducing capacity of the media/cells to be ~4 µM/ >200 µM. The relative measurement shows a ΔV_{redox} of ~200 mV spanning <100 µm between regions with and without cells (**b**, right) and demonstrates the ability to perform the titration without a reference electrode.

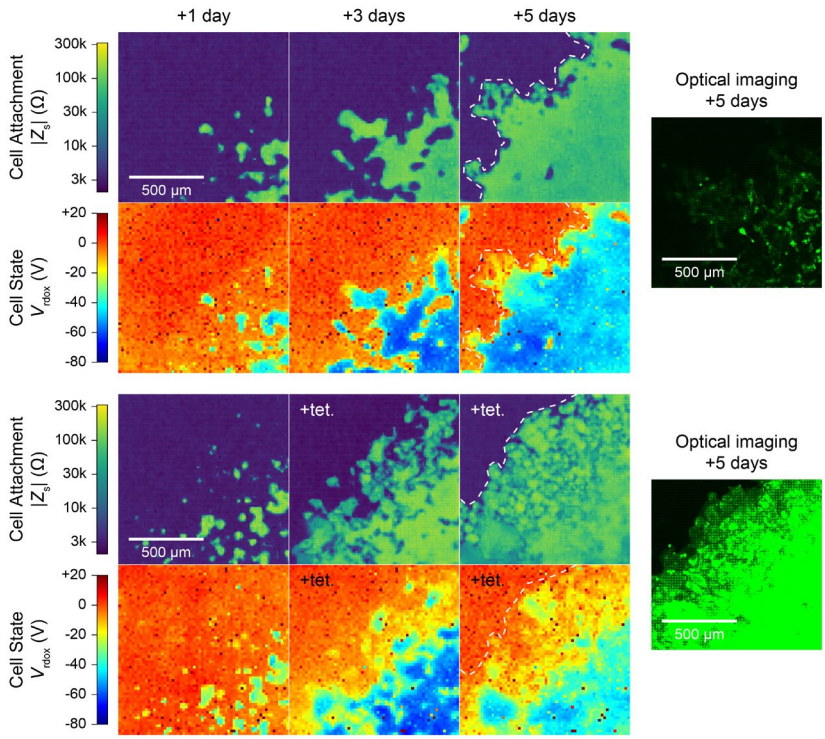

Supplementary Fig. 9 | Effects of Ras^{V12} expression on cell-substrate adhesion and the *in situ* extracellular redox potential. MDCK cells genetically modified for tetracycline-controlled Ras^{V12}, a known oncogene, and GFP expression were plated in tetracycline free media on two devices (top/bottom) with measurements made at +1, +3, and +5 days from the plating. After the +1 day measurement, tetracycline was added to one culture (bottom). Optical imaging at +5 days confirmed the bottom, tetracycline added culture was expressing the Ras^{V12}/GFP much more strongly in comparison to the top, tetracycline free culture. A significant difference in the extracellular redox potential was observed at +3 and +5 days wherein the newly grown cells on the leading edge exhibited a more positive extracellular redox potential for the Ras^{V12} expressing cells (bottom) in comparison to the non-expressing cells in the tetracycline free culture (top). A noticeable decrease in the uniformity of the tissue was also observed from the cell-substrate adhesion measurements.

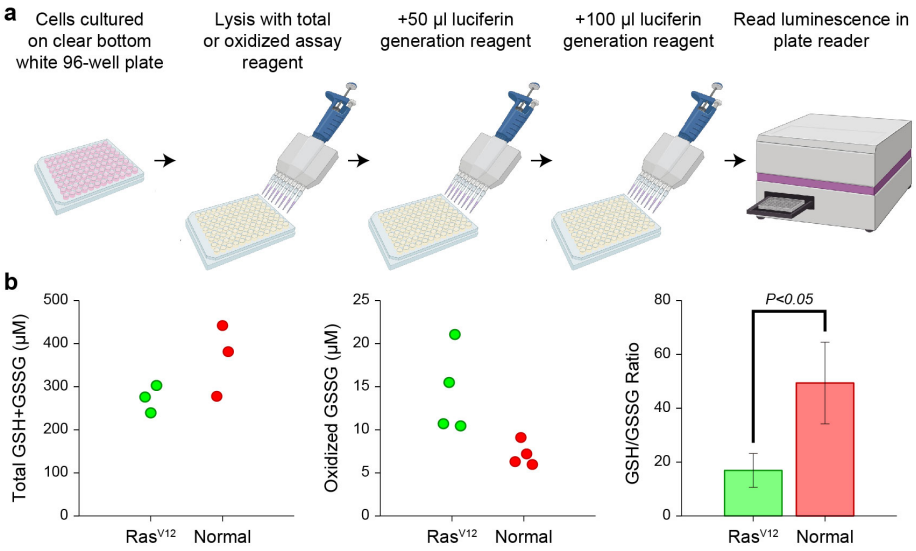

Supplementary Fig. 10 | Luminescence-based GSH/GSSG-Glo™ assay for Ras^{V12} expression comparison. a, A standard assay kit was acquired from Promega and the assay protocol was followed as outlined for both wild-type MDCK cells (normal) and Ras^{V12} expressing cells. **b,** Total GSH+GSSG measurements (left), oxidizing GSSG measurements (middle), and GSH/GSSG ratio calculations (right) for normal and Ras^{V12}-expressing MDCK cells. The ratios were calculated at 49.4 ± 15.2 for normal and 16.9 ± 6.3 for the Ras^{V12}-expressing MDCK cells (n = 3 total GSH+GSSG, n = 4 GSSG), error bars show standard deviation; P = 0.026 using n = 3.

Supplementary Discussion 1

Calculation of cell-substrate impedance, Z_s

We represent the electrode cell interface via an impedance model to describe our cell attachment and barrier measurements, see Supplementary Fig. 2e for the model schematic with definitions of the circuit components presented in the caption. Unlike other works which apply a voltage between two electrodes, to measure cell-substrate attachment, we apply a voltage from one electrode to all remaining electrodes to measure a change of cross-electrode field. This allows the field lines starting from the stimulation electrode and extending far up into the culture well to terminate on electrodes far away the stimulation. Otherwise, these field lines would need to curl back towards the adjacent electrode, increasing the amount of measured current not related to the immediate cell-electrode interface.

We model the interface using a cross-sectional type model to increase spatial resolution. If we assume $Z_s << Z_{te}$, $Z_{e,1}$, and $Z_{e,2}$, which we found to be valid for most measurements, then we can write

$$V_2 \approx \frac{1}{2}V_1 \approx \frac{1}{2}V_A \frac{2Z_s}{Z_1 + 2Z_s} \approx V_A \frac{Z_s}{Z_1} \quad (1)$$

The measured cross electrode current can also be written and expressed in terms of (1),

$$I_{12} = \frac{V_2}{Z_2} \approx V_A \frac{Z_s}{Z_1 Z_2} \quad (2)$$

To determine $Z_{e,1}$ and $Z_{e,2}$, we use the sum of the measured current across the array when the stimulus is applied to an electrode n,

$$Z_{e,n} = \frac{V_A}{I_n} \quad (3)$$

Z_s can then be solved for from (3) and (2),

$$Z_s = V_A \frac{I_{12}}{I_1 I_2} \quad (4)$$

which uses all measured currents.

To generate a high-spatial map of the Z_s, nearest neighbor cross-electrode measurements were used for each stimulation electrode: a 3×3 grid is used for each electrode (except those at the edges of the electrode array), Supplementary Fig. 2d. This creates an overall Z_s image of 190×190 pixels (in comparison to the 64 × 64 electrodes in the array). In the example, the 3×3 grid for the center electrode 5 is filled in using Z_s values corresponding to the measured currents to its nearest neighboring electrodes. Each face normalized impedance value is calculated as,

$$Z_{52} = V_A \frac{I_{52}}{I_5 I_2}, Z_{54} = V_A \frac{I_{54}}{I_5 I_4}, Z_{56} = V_A \frac{I_{56}}{I_5 I_6}, Z_{58} = V_A \frac{I_{58}}{I_5 I_8}, \quad (5)$$

where I_{xy} is the magnitude of the AC current measured by electrode y when the AC signal is applied to electrode x, and I_x [I_y] is the sum of the magnitude of the AC currents measured by all other electrodes

when the AC signal is applied to electrode *x* [*y*]. The corner normalized impedance values are then calculated as,

$$Z_{51} = \frac{V_\mathrm{A}}{\sqrt{2}}\frac{I_{51}}{I_5 I_1}, Z_{53} = \frac{V_\mathrm{A}}{\sqrt{2}}\frac{I_{53}}{I_5 I_3}, Z_{57} = \frac{V_\mathrm{A}}{\sqrt{2}}\frac{I_{57}}{I_5 I_7}, Z_{59} = \frac{V_\mathrm{A}}{\sqrt{2}}\frac{I_{59}}{I_5 I_9}, \quad (6)$$

where the square root of 2 was determined to normalize the diagonal distance of between corner electrodes. The center normalized impedance value is then determined as,

$$Z_{55} = \mathrm{median}(Z_{52}, Z_{54}, Z_{56}, Z_{58}) \quad (7)$$

The use of the cross-electrode currents not only increases the effective spatial resolution in comparison to using the max of the current distribution but it also allows for attached cells, which cause a decrease in the cross-electrode current, to be mapped, Fig. 2b. The Z_s calculation also accounts for variations in Z_e across the array, where we have sometimes observed spatial variations due to post-processing of the Pt electrodes and PtB deposition.

Calculation of transepithelial impedance, Z_{te}

To measure cell-to-cell attachment, or how well-connected cells are to each other, we can modify the stimulation protocol to measure the vertical field component, Fig. 3a. In the parallel scheme, Fig. 3a left, a voltage is applied to each electrode versus a reference with each electrode's current, $I_{te,n}$, measured, creating a vertical field in solution (the peripheral electrodes would also have a fringing field, visible in Supplementary Fig. 5c for low frequencies). Due to current needing to go through the cell sheet, the magnitude of the current will be proportional to the transepithelial impedance, Z_{te}. A second scanned scheme, Fig. 3a right, biases an electrode and its surrounding electrodes with an AC voltage and measures the current only through the center electrode. The center electrode will not pass current to surrounding electrodes as they are biased with the same signal, therefore it will only pass current due to the impedance of cell sheet above the electrode. Outside of the center and its surrounding electrodes, the remainder of the array is biased at ground to act as a current return.

In either case, the measured vertical current $I_{te,n}$ can be expressed,

$$I_{\mathrm{te,n}} = \frac{V_\mathrm{A}}{Z_{\mathrm{e,n}} + Z_{\mathrm{te}}} \quad (8)$$

Using (3), we can then solve for Z_{te},

$$Z_{\mathrm{te}} = \frac{V_\mathrm{A}}{I_{\mathrm{te,n}}} - \frac{V_\mathrm{A}}{I_\mathrm{n}} \quad (9)$$

For measurements, we determined that mid-frequencies from ~1-5 kHz are best correlated with the cell-cell connectivity (Supplementary Fig. 5). For the PtB electrodes, $Z_{e,n}$ is then sufficiently smaller than Z_{te} (Supplementary Fig. 5b) such that we estimate,

$$Z_{\mathrm{te}} = \frac{V_\mathrm{A}}{I_{\mathrm{te,n}}} \quad (10)$$

For Z_{te} experiments with just Pt electrodes, including Supplementary Fig. 7 and Supplementary Videos 5-6, the I_n measurement from the cell-substrate impedance is subtracted. Due to the scanned array measurement to calculate $Z_{te,no\ ref}$ using a 3×3 set of electrodes, the total map generated is 62×62 pixels, as the peripheral electrodes do not have neighboring biased electrodes to create the vertical field. The measurement versus the reference creates a map containing 64×64 pixels.

Supplementary Video 1 | Cell-substrate impedance maps over time showing MDCK cells settling and attaching to the surface of the CMOS electrode array, from the dataset of Fig. 2c.

Supplementary Video 2 | Cell-substrate impedance maps over time of MDCK cells where ethylenediaminetetraacetic acid (EDTA), a calcium chelator, was added to induce detachment with subsequent removal at 52 min to induce re-attachment, from the same experiment as Supplementary Fig. 3c-d.

Supplementary Video 3 | Optical fluorescent images over time during a cell patterning: a negative voltage of -1.1 V versus Ag/AgCl was applied to the whole area expect the white boxed region.

Supplementary Video 4 | Cell-substrate impedance maps over time of a wound healing assay with no drug added, from the same experiment of Fig. 2f.

Supplementary Video 5 | Multi-parametric measurements (cell-substrate impedance, transepithelial impedance, and the *in situ* extracellular redox potential) of an oxygen purge for both normal MDCK cells (upper left) and Ras^{V12} (a known oncogene) expressing MDCK cells (lower right); from the same experiment as Fig. 3c. The removal of oxygen almost eliminates the extracellular redox potential and decreases the transepithelial impedance of the normal cells due to a loss of structural polarity.

Supplementary Video 6 | Multi-parametric measurements (cell-substrate impedance, transepithelial impedance, and the *in situ* extracellular redox potential) of a Ferricyanide titration for MDCK cells show the reducing capacity of the media/cells to be ~4 µM/ >200 µM; from the same experiment of Fig. 3d-e.

Supplementary Video 7 | Cell-substrate impedance maps over time showing MDCK cells genetically modified for tetracycline-controlled Ras^{V12}, a known oncogene, growing after plating. Media with tetracycline was added after ~24 hours to turn the gene on. A significant change is observed in the uniformity of the cell-sheet and a decrease in the cell-substrate adhesion after the Ras^{V12} expression.

Supplementary Video 8 | Multi-parametric measurements (cell-substrate impedance, transepithelial impedance, and the *in situ* extracellular redox potential) of a Ferricyanide titration for both normal MDCK cells (upper left) and Ras^{V12} (a known oncogene) expressing MDCK cells (lower right); from the same experiment of Fig. 4d.